Lifetimes of negative parity states in ^{168}Er

L. Genilloud and J. Jolie
Institut de Physique, Université de Fribourg, Pérolles, CH-1700 Fribourg, Switzerland

H. G. Börner and H. Lehmann
Institut Laue-Langevin, F-38042 Grenoble Cedex 9, France

F. Bečvář and M. Krtička
Faculty of Mathematics and Physics, Charles University, CZ-180 00 Prague 8, Czech Republic

N. V. Zamfir
WNSL, Yale University, New Haven, Connecticut 06520
and Clark University, Worcester, Massachusetts 01610

R. F. Casten
WNSL, Yale University, New Haven, Connecticut 06520
(Received 3 May 2000; published 21 August 2000)

Using the GRID method the lifetimes of 12 states belonging to four negative parity bands in ^{168}Er were measured at the high flux reactor of the Institut Laue-Langevin (ILL). For $K^\pi=0_1^-$ and $K^\pi=2_1^-$ bands the absolute $E1$ transitions are in agreement with those obtained within the framework of the *sdf* IBA-1 model and their octupole vibrational character is confirmed.

PACS number(s): 21.10.Tg, 21.60.Ev, 27.70.+q, 24.10.Pa

I. INTRODUCTION

A complete set of lifetimes of nuclear excited states below 2.2 MeV in a well-deformed nucleus could form a unique database for the study of nuclear structure. A good candidate for such a nucleus is ^{168}Er, one of the best known deformed nuclei. Davidson *et al.* [1] were able to identify the bandheads of 20 rotational bands by using in a systematic way the different techniques developed for the (n,γ) reaction in combination with transfer reaction data. The development of the γ-ray induced Doppler (GRID) broadening technique afterwards gave access to the lifetimes of states populated after neutron capture [2]. In two previous GRID experiments on ^{168}Er the double gamma vibration [3] and the nature of the $K^\pi=0^+$ bands [4] have been studied. In a continuation of our prior work several low-K bands were investigated. They could be candidates for rotational bands built on the octupole vibration.

Low-lying octupole states in ^{168}Er have been first studied by Neergard and Vogel [5] and next by Cottle and Zamfir [6] who compared excitation energies and $B(E3)$ values with those given in the interacting boson approximation (IBA). Photon scattering experiments [7] provided transition probabilities of $J^\pi=1^\pm$ states, which were compared to the quasiparticle-phonon nuclear model (QPNM) [8]).

II. THE MEASUREMENTS AND THEIR RESULTS

The experiments were performed in two dedicated runs at the high flux reactor of the Institut Laue-Langevin (ILL) in Grenoble. The target consisted of natural erbium in the form of Er_2O_3 powder with its abundance of 23% in ^{167}Er. It was placed at the in-pile position 50 cm away from the reactor core where a neutron flux of 5×10^{14} n cm^{-2} s^{-1} is available. Results obtained during the two earlier experiments [3,4] on negative parity states were also reanalyzed.

A. The GRID technique

After the capture of a thermal neutron coming from the reactor, the newly formed nucleus is in an highly excited state close to the neutron separation energy. This nucleus will deexcite mostly by a cascade of γ rays. The emission of each γ ray induces a small but significant recoil to the nucleus. The subsequently emitted γ rays will be Doppler broadened rather than shifted as the directions of the initial recoils are uniformly distributed. Because the recoils are very small, $v/c<10^{-4}$, extreme precision in the detection of the γ line profile is needed. The sole instruments able to measure such a small broadening are two-axis flat crystal spectrometers like GAMS4 [9].

The experimental data measured by the instrument consist of the line shape of a γ ray. Figure 1 shows the line shape profiles for selected transitions. Two major effects combine to form this line shape, the instrument response and the Doppler broadening. The first is described by the convolution of the line shape following from the dynamical diffraction theory [10] and the small Gaussian spread, called excess width, related to imperfections of the spectrometer. The second depends on the following five effects: the temperature of the target, the decay pattern of the nucleus, the lifetimes of all intermediate levels encountered in the cascades that populate the level of interest, the slowing-down of the recoiling nucleus, and the lifetime τ of the level of interest.

Provided that all phenomena underlying the Doppler broadening are under control [2], it is evident that the life-

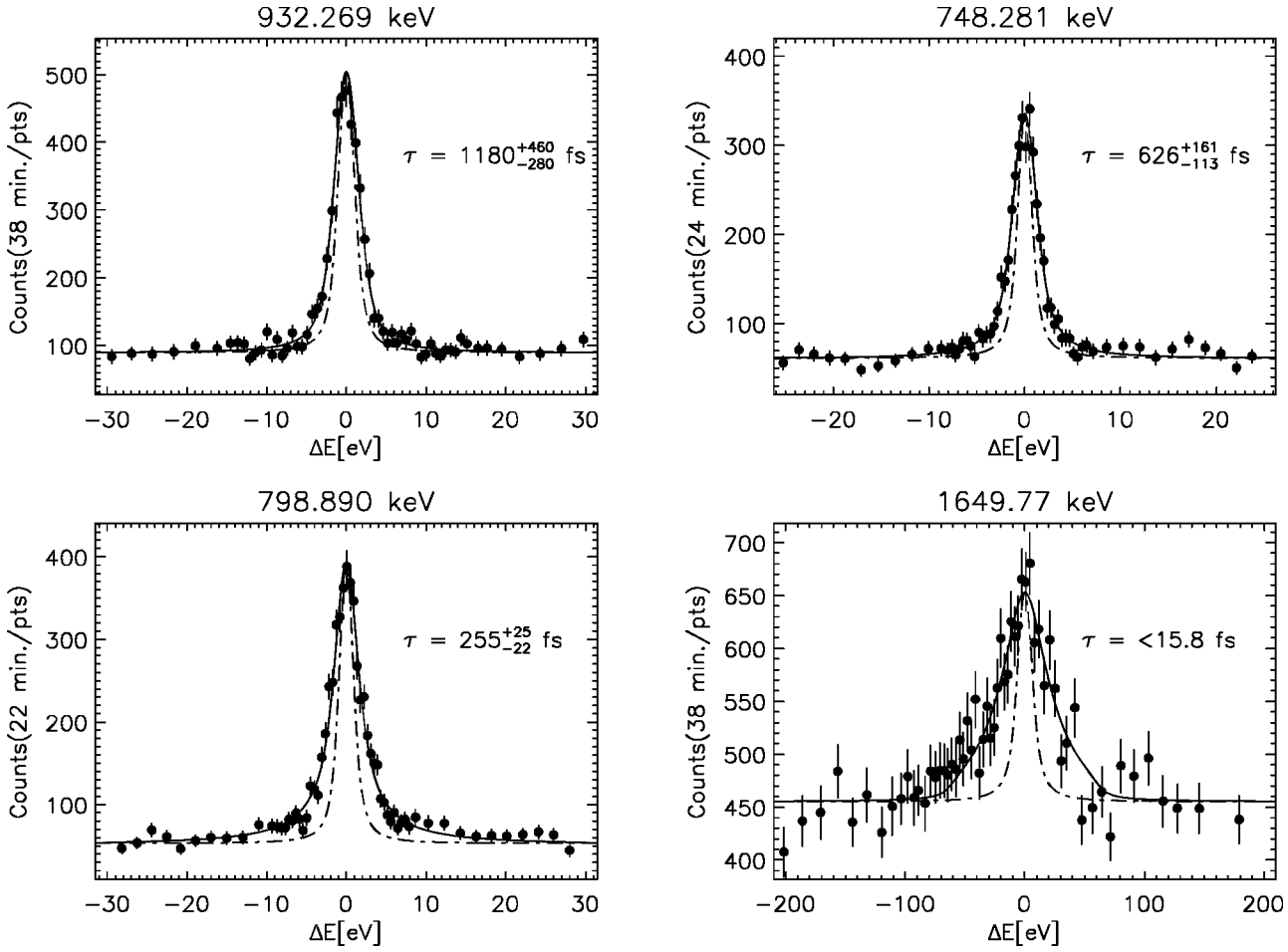

FIG. 1. Line shape of selected transitions measured with the GAMS4 spectrometer. The solid line is the fit of the γ-ray profile, the dash-dotted line corresponds to the instrumental response.

time τ can be extracted from the measured line shape. The major uncertainty in extracting lifetimes is not due directly to the measurement itself, but is related to the quantitative description of these phenomena.

Because the complete γ-decay scheme as well as the lifetimes of intermediate levels are experimentally unknown one has to base the analysis either on extreme feeding assumptions or on a statistical decay calculation. The first approach gives upper and lower limits on τ of the level of interest. To extract these limits from the measured line shape, all known feeding transitions — primaries and usually several distinct secondaries — are taken into account. By inspecting the population-depopulation balance for the level of interest the missing populating intensity is estimated. The upper limit of τ is based on the assumption that the missing intensity comes entirely from the capturing state via a sole primary transition. In this case the decaying nucleus is assumed to receive the highest possible recoil velocity from unobserved transitions. To get the lower limit, the missing intensity is attributed to hypothetical levels situated above the assumed excitation energy where the level scheme is considered to become incomplete as described in Ref. [11]. For extracting both these extreme limits of τ, all levels are assumed to be long lived, including the levels with known level energy and decay pattern. This implies that recoils occurring prior to the depopulation of these specified levels are not assumed to contribute to Doppler broadening of a γ line under the study.

With these assumptions one can predict the nuclear velocity distribution at the moment when the level of interest is populated. Knowing this distribution, the slowing down of the atom is then treated in the framework of mean free-path approach (MFPA) to predict the corresponding line shape as discussed in Ref. [2]. Comparing these line shapes with the observed profile the lower and upper limits are in turn estimated.

B. Statistical simulation of γ-ray cascades

In the second approach the lifetime estimates were deduced with the aid of *joint simulations* of both participating phenomena, specifically γ cascades that are responsible for the nuclear recoils, as well as slowing-down of the deexciting nucleus due to atomic collisions. These simulations were performed to cover the time interval initiated by the emission of a primary γ ray and ending at the moment of the depopulation of the level of interest.

Assuming the validity of the statistical model of the nucleus and the paradigm of the photon strength functions (PSFs) the algorithm DICEBOX [12,13] is used to generate γ cascades by the Monte Carlo method. With this algorithm a

full set of level energies, branching intensities and total radiation widths is generated using the technique of precursors, as explained in Ref. [12]. This set, called hereafter a nuclear realization, characterizes decay properties of a complete level system. It is understood that there exists an infinite number of nuclear realizations, one of them being identical with the real nucleus. Having a fixed nuclear realization, independent cascade decays of the neutron capturing state are repeatedly simulated with the algorithm DICEBOX. Each such trial yields energies of the individual γ rays of a given cascade. Knowing the total radiation widths of the intermediate levels involved, emission times of the individual γ-rays of each cascade are easily calculated. The interval between any pair of successive emissions is considered to be a quantity drawn at random from the corresponding exponential distribution, whose lifetime parameter is uniquely determined by the total radiation width of an encountered intermediate level. In total 20 nuclear realizations have been simulated and for each of them 50 000 cascades were produced.

The semiempirical expression for the PSF of $E1$ radiation proposed in Ref. [14] was adopted for these simulations. In acceptable agreement with the systematics in Ref. [15] values $k_0=3$ and $E_{\gamma 0}=4.5$ MeV for parameters entering this expression were chosen. In the case of $M1$ radiation it was assumed that the photon strength comes from the scissors and spin-flip resonances. In conformity with the NRF data [7] and with the data on the excited-state scissors resonances, see Refs. [16,17], the integrated scissors-resonance strength was taken to be $\Sigma B(M1)\uparrow = 4.1\ \mu_N^2$ for the γ-ray energy interval of 2–4 MeV, while in the case of the spin-flip resonance we assumed a total integrated strength of $\Sigma B(M1)\uparrow = 11.5\ \mu_N^2$. Concerning $E2$ radiation, an energy-independent photon strength of $k_{E2}=1\times 10^{-10}$ MeV^{-5} was postulated. The level density was described by the Bethe formula. As shown in Ref. [13], careful selection of the models for PSFs and the level density is crucial for achieving a minimum bias in estimating lifetimes of short-lived levels with $\tau < 100$ fs.

In the above-mentioned joint simulations the atomic collisions responsible for slowing-down are treated in the framework of the fluctuating free path approach (FFPA) [13]. Most of the assumptions on which the FFPA is based are identical to those of MFPA. The differences between the approaches are as follows: (i) the path between collisions within FFPA is considered to be a random realization of an exponential distribution, whose average is adjusted to the *mean free path* at a given velocity, (ii) in the case of FFPA the thermal motion of atoms in the sample is taken into account during the whole process of γ emission and atomic collisions, affecting in this way the mean free path, while in the case of MFPA the contribution of thermal motion is applied only after the moment when the slowing-down atom reaches the thermal velocity, and (iii) in FFPA the relative energy losses during atomic collisions are considered to be variable. It should be stated that the FFPA yields — in the case of the same feeding pattern — lifetime values are reduced compared to those from statistical calculations using the MFPA, being in agreement with results from other methods (DSAM, RMD), see Ref. [18].

TABLE I. Instrumental response for the different runs.

Run	Date	Excess width [marcsec]	Thermal velocity [m/sec]	Transitions measured [keV]
1	7.1990	6.2(1)	311(11)	1942.7
2	4.1995	13.3(2)	325(24)	1706.4
3	2.1998	9.9(3)	428(25)	798.9,932.7,1279.1,1649.8
4	5.1998	8.4(3)	497(21)	737.7,748.3,790.0 980.0,1892.6,1921.1

C. Experimental results

As has been mentioned above the temperature of the target material contributes also to the broadening of the line profile. This was determined in the usual manner [2] by measuring the broadening of a γ transition depopulating a long-lived state. The instrumental response — given by dynamical diffraction theory folded with a tiny Gaussian spread called excess width — was deduced from nondispersive scans. The values obtained are given in Table I for the different runs. More details concerning these procedures may be inferred from Ref. [2].

The measured line profiles including the contribution from the instrumental response and thermal width are shown in Fig. 1 for selected transitions, while Fig. 2 shows the scans of the χ^2 surface as a function of the lifetime. The resulting lifetime corresponds to the minimum of the function interpolating the curve, whereas the errors are given by the values for τ at $\chi^2_{\min}+1$. When the form of the interpolating function is parabolic the errors are quasisymmetric.

The lifetimes have been extracted with both approaches, MFPA with extreme limit assumptions and FFPA using simulations of the γ-ray cascades; they are given in Table II together with the deduced $B(E1;J_i\rightarrow J_f)$ values. Of the lifetimes measured in this work, one (the 1786.1 keV level) can be compared with the result from another experiment, i.e., the nuclear resonance fluorescence (NRF) measurement. Using the FFPA description a longer lifetime is found. Nevertheless, in view of the relatively large uncertainties these values are not inconsistent.

In addition to the data on the negative-parity bands the data from two previous measurements [3,4] on the $K^\pi=4^+$ double-γ band and $K^\pi=0^+$ bands were reanalyzed (see lines 2 and 3 in Table III) using the FFPA and the DICEBOX simulations. The χ^2 plot for the decay of the $2^+_{K^\pi=0^+_2}$ state is given in Fig. 2.

III. COMPARISON WITH CALCULATIONS

An octupole vibration about a spherical shape creates an excited state with $J^\pi=3^-$. In deformed nuclei this octupole state is split into four intrinsic states with $K^\pi=0^-,1^-,2^-,3^-$, K being the absolute value of the projection of the octupole phonon angular momentum on the symmetry axis of the nucleus. On each of these states, a rotational band is built. The candidates for such a structure in ^{168}Er are shown in Fig. 3. The uncertainties in the assignment of the

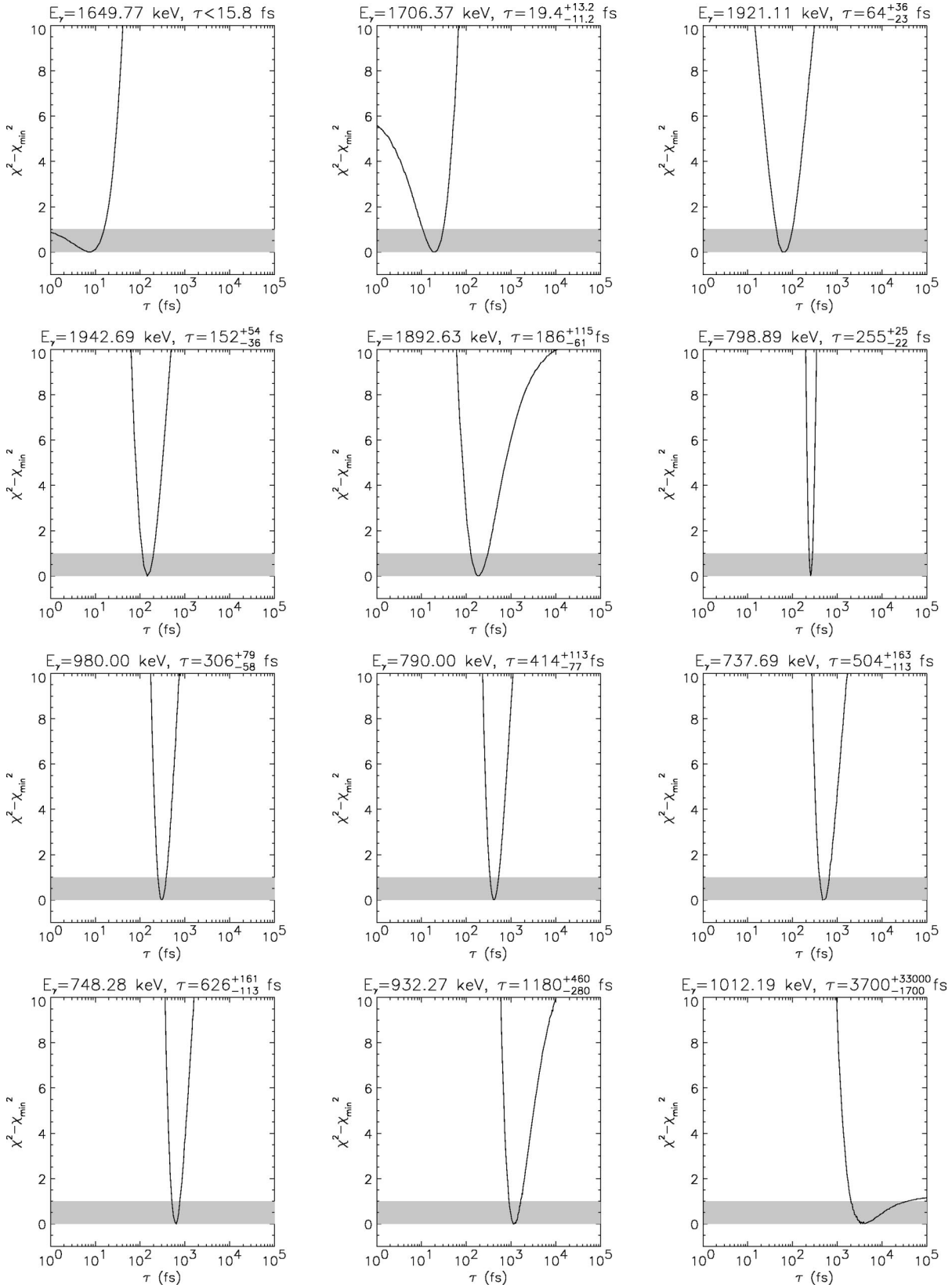

FIG. 2. χ^2 plots for the different measured γ rays as a function of the lifetime τ. The gray areas represent the regions below the one-σ limit.

TABLE II. Experimental and calculated absolute $B(E1)$ strengths.

	Level			Lifetime [fs]				$B(E1;J_i\rightarrow J_f)$ [m W.u.]				
K^π	J_i^π	E_x [keV]	E_γ [keV] [a]	τ_{FFPA} [b]	τ_{ext} [c]	τ_{litt} [e]	J_f^π	Exp. [f]	Calc.		E_{th} [keV]	
									SDF	QPNM [g]	SDF	QPNM [g]
0_1^-	1^-	1786.1	1706.37	$19.4^{+13.2}_{-11.2}$	<137	5.0(6)	0_1^+	1.13^{+150}_{-46}	0.881	2.94	1807	1850
							2_1^+	1.97^{+270}_{-80}	1.645			
	3^-	1913.9	1649.77	<15.8	7–69		2_1^+	0.34–3.3 [d]	1.057		1893	
							4_1^+	0.57–5.6 [d]	1.137			
	5^-	2185.1	1921.11	64^{+36}_{-23}	14–228		4_1^+	0.43^{+24}_{-16}	0.982		2094	
							6_1^+	0.35^{+20}_{-13}	0.698			
1_1^-	1^-	1358.9	1279.127		$\geqslant 7000$		0_1^+	<0.0054	0.013	0.98	1259	1300
							2_1^+	<0.0153	0.067			
							2_2^+	<0.0021	0.035			
	3^-	1431.5				$5.9\cdot10^4$	2_1^+	0.0011	0.181		1380	
							4_1^+	0.0017	0.282			
							3_1^+	0.0001	0.002			
1_2^-	1^-	1936.6				346(101)	0_1^+	0.108^{+44}_{-24}	0.008	0.233	2178	1920
							2_1^+	0.020^{+8}_{-5}	0.052			
	2^-	1972.3	1892.63	186^{+115}_{-61}	95–570		2_1^+	0.137^{+67}_{-52}	0.006		2218	
							2_2^+	0.134^{+65}_{-51}	0.033			
							3_1^+	0.471^{+230}_{-180}	0.000			
	3^-	2022.3	1942.69	152^{+54}_{-36}	<458		2_1^+	0.215^{+67}_{-56}	0.045		2379	
							4_1^+	0.082^{+25}_{-21}	0.121			
	4^-	2097.6	979.996	306^{+79}_{-58}	<560		4_1^+	0.063^{+15}_{-13}	0.014		2422	
							3_1^+	0.153^{+36}_{-31}	0.054			
							4_2^+	0.047^{+11}_{-9}	0.042			
							5_1^+	0.326^{+76}_{-67}	0.012			
2_1^-	2^-	1569.5	748.281	626^{+161}_{-113}	415–1166		2_1^+	0.0060^{+13}_{-12}	0.010		1616	
							2_2^+	0.815^{+180}_{-170}	0.988			
							3_1^+	0.493^{+110}_{-100}	0.469			
	3^-	1633.5	737.686	504^{+163}_{-113}	239–1181		2_2^+	0.397^{+110}_{-97}	0.339		1700	
							3_1^+	0.631^{+180}_{-150}	0.583			
							4_2^+	0.652^{+190}_{-160}	0.639			
3_1^-	3^-	1541.6				$1.15\cdot10^4$	2_2^+	0.021			-	
							3_1^+	0.009				
							4_1^+	0.010				
3_2^-	3^-	1828.1	932.269	1180^{+460}_{-280}	750–2890		2_2^+	0.029^{+9}_{-8}				
							3_1^+	0.159^{+50}_{-45}				
							4_2^+	0.140^{+44}_{-39}				
	4^-	1892.9	798.890	255^{+25}_{-22}	47–441		3_1^+	0.0220(20)				
							5_1^+	0.0302(28)				
	5^-	1983.0	790.001	414^{+113}_{-77}	<1069		6_2^+	0.0377^{+86}_{-81}				

[a] Transition measured for the corresponding level.
[b] Lifetime determined using DICEBOX [12] simulations for unknown feeding and FFPA for atomic collisions.
[c] Lifetime determined using extreme assumptions for the unknown feeding [11].
[d] $B(E1)$ values calculated using τ_{ext} because of nonconvergence of τ_{FFPA} in the fit.
[e] Lifetime taken from Ref. [19].
[f] Computed with τ_{FFPA} and branching ratios taken from Ref. [1].
[g] Values calculated in the quasiparticle-phonon nuclear model (QPNM) (Ref. [8]).

$K^\pi=1^-$ and $K^\pi=3^-$ bands as octupole vibrational come from the observation of significant two-quasiparticle strength to the lower levels in single-neutron stripping reactions [20]. In order to settle the question of the structure of these bands, it is necessary to get information of the structure of the wave functions; this can be done considering the electromagnetic transition probabilities.

The negative parity states can be described in the IBA-1 model [21] by adding a single f boson with $L=3$ to the usual sd boson model space [22,23]. The sdf Hamiltonian is

TABLE III. Comparison between lifetimes extracted with FFPA and previous approaches.

J^π_K	E_γ [keV] [a]	$\tau_{\rm stat}$ [fs] [b]	Ref.	$\tau_{\rm FFPA}$ [fs]	$\tau_{\rm litt}$ [fs] [c]
$1^-_{1^-}$	1706.37	$22.7^{+12.5}_{-9.8}$	This work	$19.4^{+13.2}_{-11.2}$	5.0(6)
$2^+_{K^\pi=0^+_2}$	1012.19	2900^{+3100}_{-1000}	[4]	3700^{+33000}_{-1700}	
$4^+_{\gamma\gamma}$	1234.76	440^{+90}_{-70}	[3]	470^{+105}_{-76}	320(16)

[a]Transition measured for the corresponding level.
[b]Statistical model using MFPA to describe the slowing down.
[c]Lifetime taken from Ref. [19].

$$H = H_{sd} + H_f + V_{sdf}, \tag{1}$$

where the different terms were proposed in [6,24]. For the calculation of energies we used the same parameters as those used in Ref. [6]. The results are discussed in the next paragraph. The $E1$ transition rates were calculated using the operator $T^{(E1)}_{sdf}$ defined in Ref. [6] with the same parameters with the exception of the effective charge for which we adopted the value $e_1 = 0.136$ e fm, half the value used in Ref. [6].

The agreement of the calculated $B(E1)$ values with the data is very good (see Table II) for the $K^\pi = 0^-_1$ and $K^\pi = 2^-_1$ bands. This fact is in line with the octupole vibrational interpretation of these 2 bands. In the case of the $K^\pi = 1^-_1$ and $K^\pi = 1^-_2$ bands the overall agreement is rather poor. However, Table II shows that most experimental and calculated $B(E1)$ values from these bands, at least to the ground band, are much smaller than those from the $K^\pi = 0^-_1$ and $K^\pi = 2^-_1$ bands. Therefore, these transitions presumably proceed by noncollective amplitudes and one would not expect good agreement from a collective model such as the IBA. We do note, however, that the $K^\pi = 1^-_2$ band is very well reproduced in the QPNM calculations, both in energy and $B(E1)$ values (see Table II). In order to see the degree of collectivity of different octupole bands, we compare in Table IV the experimental $B(E3;0_{\rm g.s.} \rightarrow 3^-)$ values from Ref. [25] with the IBA results using the $T(E3)$ operator defined in Ref. [6] ($e3 = 0.076$ $e\,{\rm b}^{3/2}$, $\chi_3 = 0.76$). The calculated $B(E3)$ values agree very well with the data for $K^\pi = 1^-_1, 2^-_1, 0^-_1$. The IBA model predicts a very small value for $B(E3;0_{\rm g.s.} \rightarrow 3^-_{K^\pi=1^-_2})$, in agreement with the fact that this state was not observed in the inelastic scattering experiment [25]. The very small value predicted by IBA, which is obviously a collective model, indicates that a small $B(E3;0_{\rm g.s.} \rightarrow 3^-)$ value is not always an argument for lack of collectivity. In the present case, the $K^\pi = 1^-_2$ band and, as will be seen in the next section the $K^\pi = 3^-_1$ band, are octupole excitations based on the γ band and not on the ground state. This situation is reminiscent of the case for the $K^\pi = 0^+_2$ band which, in the IBA, has strong $B(E2)$ values to the γ band but nearly vanishing ones to the ground band: it is a collective band, but collectively related to the γ band not the ground band.

TABLE IV. Comparison between experimental $B(E3;0^+_{\rm g.s.} \rightarrow 3^-)$ values (from Ref. [25]) with SDF-IBA-1.

K^π	$E_{\rm exc}(J^\pi = 3^-)$ [keV]		$B(E3;0^+_{\rm g.s.} \rightarrow 3^-)$ [$e^2\,{\rm b}^3$]	
	Exp.	Calc.	Exp.	Calc.
1^-_1	1431	1380	0.046(5)	0.051
2^-_1	1633	1700	0.058(6)	0.035
0^-_1	1913	1893	0.023(3)	0.015
1^-_2	2022	2379		0.003
3^-_1	1541		0.003(1)	
3^-_2	1828		0.007(2)	
3^-_3	1999		0.005(1)	
3^-_4	2323		0.018(2)	
3^-_5	2337 [a]			
3^-		2253		0.000

[a]Taken from Ref. [26].

IV. DISCUSSION

The $B(E1)$ data confirms the results of Refs. [5,6] that the $K^\pi = 0^-_1$ and 2^-_1 bands are octupole vibrational excitations based on the ground state. The $B(E3)$ data show that the $K^\pi = 1^-_1$ band has the same character. The situation with the $K^\pi = 3^-$ bands is more complicated. There are five experimental $K^\pi = 3^-$ bands at 1541, 1828, 1999, 2323, and 2337 keV and the lowest $K^\pi = 3^-$ band predicted by the IBA model is at 2253 keV (see Table IV). For the first three the experimental $B(E3;0_{\rm g.s.} \rightarrow 3^-)$ values are very small. The IBA model predicts an extremely small $B(E3;0_{\rm g.s.}$

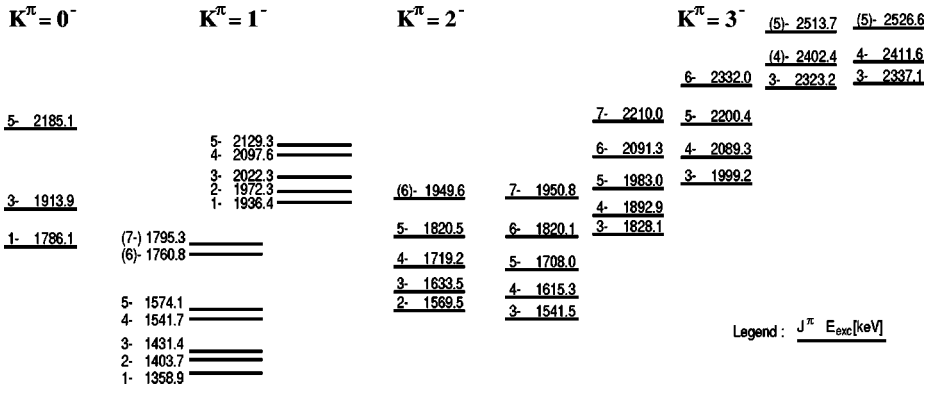

FIG. 3. Candidates for rotational bands built on the octupole vibration.

TABLE V. The IBA $E3$ squared reduced matrix elements.

K^π	$E_{exc}(J^\pi=5^-)$ [keV] (th.)	$M(E3;2_i^+\rightarrow 5^-)^2$ [e^2b^3] 2_1^+ (g.s.)	2_2^+ (γ band)
1_1^-	1598	**0.125**	0.003
2_1^-	1945	**0.047**	0.009
0_1^-	2094	**0.042**	0.001
1_2^-	2698	0.004	**0.025**
3_1^-	2487	0.000	**0.047**

$\rightarrow 3^-_{K^\pi=3_1^-}$) value, as well. However, the existing data do not permit one to identify which experimental $3^-_{K^\pi=3^-}$ state corresponds to $3^-_{K^\pi=3_1^-}$ in the IBA. Moreover, the IBA predictions for the $B(E1)$ values related to the $K^\pi=3_1^-$ band are considerably smaller than the experimental $B(E1)$ values corresponding to the $K^\pi=3_1^-$ and 3_2^- bands. The fact that the IBA predictions do not fit these data suggests a noncollective character of these bands and it is possible that the $K^\pi=3^-$ octupole vibrational band is the $K^\pi=3_3^-$ band or higher, but there are currently no definitive experimental data available. In order to understand better the structure of the $K^\pi=1_2^-$ and 3_1^- bands predicted in the IBA model we compare in Table V the squared reduced matrix elements $M(E3)^2$ calculated for transitions between 2_1^+, 2_2^+, and 5^- states of different bands. The use of the reduced matrix elements is prefered because the statistical factor $2J_i+1$ is removed, allowing a direct comparison with the $B(E3;0^+_{g.s.}\rightarrow 3^-)$ values. The corresponding $B(E3;2_i^+\rightarrow 5^-)$ values are shown in Fig. 4. The squared reduced matrix elements for the transitions from the 2_1^+ state to the 5^- members of the $K^\pi=0_1^-$, 1_1^-, and 2_1^- bands are comparable with the calculated $B(E3)$ values from $0^+_{g.s.}$ to their 3^- members (see Table IV). The reduced matrix elements for the transitions from the 2_2^+ state to the same 5^- states are very small. Thus, these predictions reflect the character of these bands as octupole vibrations built on the ground state. However, in the case of the $K^\pi=1_2^-$ and 3_1^- bands the situation is reversed: these bands are calculated to have large reduced matrix elements to the γ band and not to the ground state, indicating that these two bands are octupole vibrations built on γ vibrations, and hence have a two-phonon (quadrupole-octupole) character.

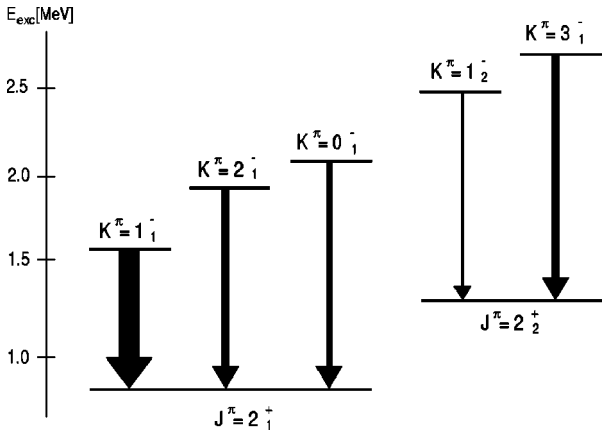

FIG. 4. Largest theoretical $B(E3;5^-\rightarrow 2_i^+)$ strength to the 2_1^+ and 2_2^+ states from various negative parity bands in ^{168}Er in the IBA. In each case, the transition to the other 2^+ state is calculated to be about an order of magnitude weaker.

V. CONCLUSIONS

The lifetimes of 12 states in four negative parity bands ($K^\pi=0_1^-$, 1_1^-, 1_2^-, 2_1^-, and 3_2^-) in ^{168}Er were measured using the GRID method, giving this nucleus one of the best known sets of negative parity states. The IBA model reproduces very well the $B(E1)$ values, the excitation energies and the $B(E3)$ values for the $K^\pi=0_1^-$ and 2_1^- bands. It fails to reproduce the $B(E1)$ values related to the $K^\pi=1_1^-$ and $K^\pi=1_2^-$ bands. However, the excitation energies and the $B(E3)$ values support the octupole vibrational character of these bands, based on ground state and on γ vibration, respectively. The $B(E1)$ values related to the $K^\pi=3_2^-$ band are not reproduced by the model and probably this band does not have a collective character. The IBA calculations indicate that the collective $K^\pi=3^-$ band is located higher in energy and it is a double phonon (quadrupole γ + octupole) excitation, similar to the $K^\pi=1_2^-$ band.

ACKNOWLEDGMENTS

This work was supported by the Swiss National Science Foundation and U.S. DOE under Contract Nos. DE-FG02-91ER40609 and DE-FG02-88ER40417.

[1] W.F. Davidson, D.D. Warner, R.F. Casten, K. Schreckenbach, H.G. Börner, J. Simić, M. Stojanović, M. Bogdanović, S. Koički, W. Gelletly, G.B. Orr, and M.L. Stelts, J. Phys. G **7**, 455 (1981); **7**, 843(E) (1981).
[2] H.G. Börner and J. Jolie, J. Phys. G **19**, 217 (1993).
[3] H.G. Börner, J. Jolie, S.J. Robinson, B. Krusche, R. Piepenbring, R.F. Casten, A. Aprahamian, and J.P. Draayer, Phys. Rev. Lett. **66**, 691 (1991); **66**, 2837(E) (1991).
[4] H. Lehmann, J. Jolie, F. Corminboeuf, H.G. Börner, C. Doll, M. Jentschel, R.F. Casten, and N.V. Zamfir, Phys. Rev. C **57**, 569 (1998).
[5] K. Neergard and P. Vogel, Nucl. Phys. **A145**, 33 (1970).
[6] P.D. Cottle and N.V. Zamfir, Phys. Rev. C **54**, 176 (1996).
[7] H. Maser, S. Lindenstruth, I. Bauske, O. Beck, P. von Brentano, T. Eckert, H. Friedrichs, R.D. Heil, R.-D. Herzberg, A. Jung, U. Kneissl, J. Margraf, N. Pietralla, H.H. Pitz, C. Wesselborg, and A. Zilges, Phys. Rev. C **53**, 2749 (1996).
[8] V.G. Soloviev, A.V. Sushkov, and N.Yu. Shirikova, Phys. Rev. C **56**, 2528 (1997).
[9] E.G. Kessler, G.L. Greene, M.S. Dewey, R.D. Deslattes, H.G.

Börner, and F. Hoyler, J. Phys. G **14**, S167 (1988).
[10] W.H. Zachariasen, *Theory of X-ray Diffraction in Crystals* (Wiley, New York, 1945).
[11] H.G. Börner, M. Jentschel, N.V. Zamfir, R.F. Casten, M. Kritcka, and W. Andrejtscheff, Phys. Rev. C **59**, 2432 (1999).
[12] F. Bečvář, Nucl. Instrum. Methods Phys. Res. A **417**, 434 (1998).
[13] F. Bečvář, M. Krtička, and M. Jentchel, *Applications of High-Precision γ-spectroscopy* (Notre Dame University Press, South Bend, IN 1998).
[14] J. Kopecky, M. Uhl, and R.E. Chrien, Phys. Rev. C **47**, 312 (1993).
[15] J. Kopecky, ''Handbook for calculations of nuclear reaction data,'' Reference input parameter library, IAEA-TECDOC-1034, August, 1998 (unpublished), p. 97.
[16] F. Bečvář, P. Cejnar, J. Honzátko, K. Konečný, I. Tomandl, and R.E. Chrien, Phys. Rev. C **52**, 1278 (1995).
[17] F. Bečvář, M. Krtička, J. Honzátko, I. Tomandl, F. Käppeler, F. Voss and K. Wisshak, in 10th Capture Gamma-Ray Spectroscopy and Related Topics, Santa Fe, 1999 (in press).
[18] J. Keinonen, in *Workshop on Application of High Resolution Gamma Spectroscopy in Studies of Atomic Collisions and Nuclear Lifetimes*, edited by H.G. Börner, J. Jolie, M. Pendlebury, and S. Ulbig (Institut Laue-Langevin, Grenoble 1992), p. 131.
[19] V.S. Shirley, Nucl. Data Sheets **53**, 223 (1988).
[20] D.G. Burke, B.L.W. Maddock, and W.F. Davidson, Nucl. Phys. **A442**, 424 (1985).
[21] F. Iachello and A. Arima, *The Interacting Boson Model* (Cambridge University, Cambridge, 1987).
[22] A. Arima and F. Iachello, Phys. Lett. **57B**, 39 (1975).
[23] A. Arima and F. Iachello, Ann. Phys. (N.Y.) **111**, 201 (1978).
[24] A.F. Barfield, J.L. Wood, and B.R. Barrett, Phys. Rev. C **34**, 2001 (1986); A.F. Barfield, B.R. Barrett, J.L. Wood, and O. Scholten, Ann. Phys. (N.Y.) **182**, 344 (1988).
[25] I.M. Govil, H.W. Fulbright, D. Cline, E. Wesolowski, B. Kotlinski, A. Backlin, and K. Gridnev, Phys. Rev. C **33**, 793 (1986).
[26] W.F. Davidson and W.R. Dixon, J. Phys. G **17**, 1683 (1991).